ELSEVIER

Marine Geology 182 (2002) 161–177

MARINE GEOLOGY
INTERNATIONAL JOURNAL OF MARINE GEOLOGY, GEOCHEMISTRY AND GEOPHYSICS

www.elsevier.com/locate/margeo

Sediment facies determination using acoustic techniques in a shallow-water carbonate environment, Dry Tortugas, Florida

Donald J. Walter *, Douglas N. Lambert, David C. Young

Naval Research Laboratory, Marine Geosciences Division/Code 7431, Stennis Space Center, MS 39529, USA

Received 11 June 1999; accepted 16 April 2001

Abstract

Two high-frequency acoustic seafloor classification systems (12- and 15-kHz) were used in conjunction with sediment core analysis to characterize sediment facies at a study site near Garden Key in Dry Tortugas, Florida. The acoustic system uses echo return amplitude to compute acoustic impedance that is then correlated with sampled sediment impedance values calculated from wet bulk density and compressional wave velocity. Several bottom provinces were identified using the 15-kHz data to construct a real-time map of ship tracks in colors that represent the surficial sediment facies type. Sediment facies over the entire study site (36 km^2) range from sandy silts to exposed limestone rock and coral reef structures. Color contour maps using the 12-kHz data, created after correlating acoustic impedance predictions with core measured sediment properties, validates the initial facies pattern predictions made in real-time. The sediment facies patterns indicate a long-term pattern of deposition of fine-grained, silt-sized, surficial sediments in an area adjacent to the emergent carbonate embankment. Two-dimensional acoustic profiles along survey tracklines also provide cross-sectional views of seafloor and subbottom stratigraphy that confirm the buildup of these fine sediments in the northwest corner of the study site. A generous supply of sediment resulting from an abundance of benthic green algae (*Halimeda* sp.) on adjacent shallow platforms form a thick sequence of fine sandy silt at the base of the southeastern edge of the embankment and fringing reef. Sediment cover over the limestone bedrock thins and becomes coarse southeast of Garden and Bush Keys, suggesting the likely existence of a dominant flow around the shallow carbonate embankment that restricts export of fine sediments out of the area. Published by Elsevier Science B.V.

Keywords: Acoustic methods; Acoustic surveys; Bottom mapping; Seafloor characterization; Sediment classification; Sediment facies; Remote sensing techniques

1. Introduction

Terminology used to describe carbonate rock and sedimentary facies is quite elaborate and can be rather confusing. Neither established carbonate rock classifications or carbonate grain type descriptors provide a satisfactory correlative that can be easily used to characterize surficial sediments with digital acoustic data. These complex terminologies are commonly employed after rigorous analysis of directly sampled sedimentary units (Dunham, 1962; Bathurst, 1975; Enos,

* Corresponding author.
Tel.: +1-228-688-5478; Fax: +1-228-688-5752.
E-mail address: don.walter@nrlssc.navy.mil (D.J. Walter).

0025-3227/02/$ – see front matter Published by Elsevier Science B.V.
PII: S0025-3227(01)00233-X

1974; Folk, 1974/1980; Davis, 1983). Standard methods of sediment analysis for physical (grain size, porosity, density), geotechnical (shear strength) and acoustic (sound speed, attenuation) properties are also labor and time intensive. Likewise, direct sampling of bottom and subbottom sediments requires large quantities of samples and high spatial sampling densities that require substantial time, effort and energy to adequately sample an area of interest. These limitations place significant constraints on the capability to generate sediment province maps and other graphical or analytical products in near real-time either during or shortly after completion of a geologic study.

The acoustic method, although not as detailed in sedimentologic terms and somewhat qualitative, can provide near-immediate graphic output for timely assessment of surficial sediment facies during a survey (Lambert et al., 1993; Mallinson et al., 1997; Walter et al., 1997; Walter, 1998). Although ground truth sediment samples are still required, they can be obtained more rapidly because fewer samples are needed. Furthermore, the sampling sites can be more tactfully selected because the acoustic data provide a guide for selection of sample sites.

We have developed a technique, using a high-frequency subbottom profiler, whereby the returned acoustic intensity is utilized to calculate the acoustic impedance of the surficial sediment. This data is combined with ship position information to create a map of ship tracks colored according to the calculated sediment acoustic impedance. This real-time map is used to delineate and characterize sediment provinces in a study site adjacent to Garden Key, Dry Tortugas, Florida. Ground truth sediment core or grab samples from each of the provinces were used to validate the sediment provinces characterized by the acoustic data.

The primary objectives of this paper are to characterize the sediment facies type and develop a representative description of the seafloor morphology in Southeast Channel, Dry Tortugas, Florida and to describe the acoustic techniques used to define and classify these sediments and sediment provinces.

2. Physical setting

The Dry Tortugas are a group of islands situated near the southwest corner of the Florida Platform approximately 130 km west of Key West, Florida. The study site is located in Southeast Channel, south and slightly east of Garden and Bush Keys (Fig. 1) within Dry Tortugas National Park (Murphy, 1993). The Gulf of Mexico borders the area on the north and the Straits of Florida are directly to the south. The site is well protected from seasonal storm activity, which generally approaches from the north and northwest, by the shallow carbonate platform that underlies the subaerially exposed keys to the west and north. The protection afforded by the carbonate banks results in thick accumulations (approximately 2–5 m), of sediments in assorted combinations of silt, sand, and shell in several depositional zones within the study site. Tropical cyclone activity during the summer and fall (Ford et al., 1988) may also influence sediment distribution patterns in, and adjacent to the experimental site. These major, but short-lived, events can cause significant loss of living coral reef structure that may form storm deposits of coarse coral and shell debris (Shinn et al., 1990; Mallinson et al., 1997; Stephens et al., 1997). Depending on current flow near and around the carbonate banks or reefs, fine carbonate sediments can either be transported out of the area or deposited in areas of impoundment where current speeds drop rapidly to allow deposition of the fine sediment. Although tidal range in the Dry Tortugas during spring is only 0.52 m (Sturges, 1993), high current flows exist in narrow channels in the region. These flows slacken between tides even during high-flow spring-tide conditions to allow unhindered diving (Sturges, 1993). Current measurements made to the west of the Dry Tortugas (Science Applications, 1987) indicate a dominant north/northeast flow at a maximum rate of < 0.10 m/s having cyclic reversals to the south/southwest at times in excess of 0.10 m/s. Wright et al. (1997) reported a net flow during a month-long experiment of 0.047 m/s in a south-southwest direction (215°) at a site in the northwest corner of the study area. Shinn et al. (1982) report a north–south

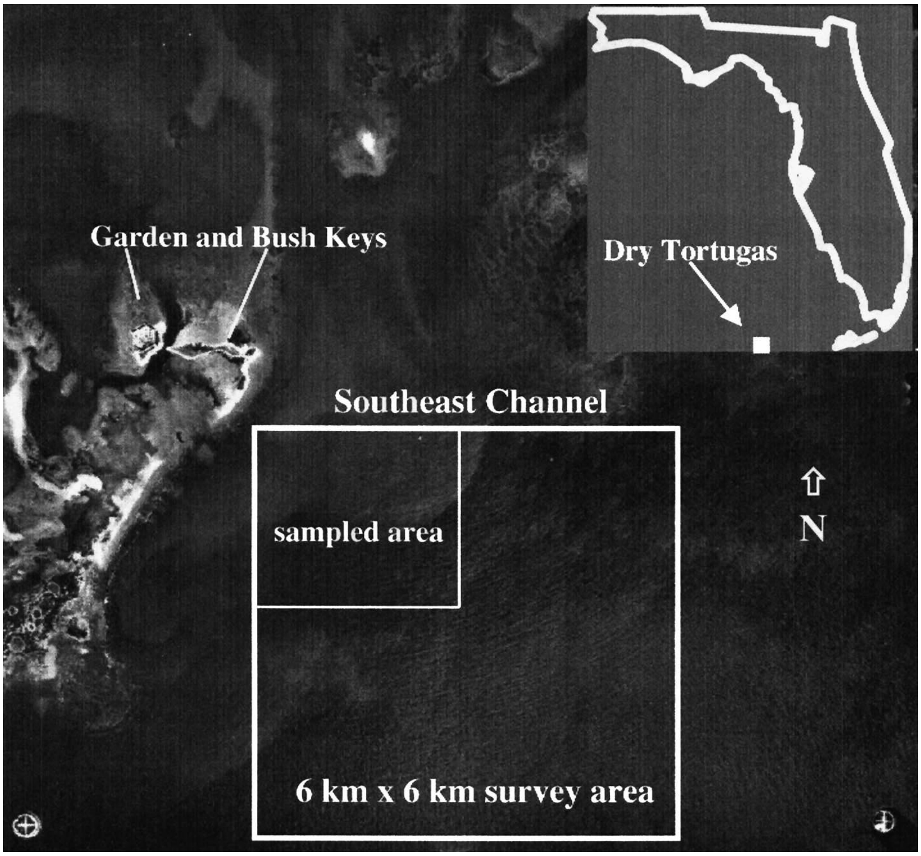

Fig. 1. Upper right box shows location of Dry Tortugas relative to Florida Peninsula and Lower Florida Keys. Aerial photo image of Southeast Channel, Dry Tortugas, Florida in lower center and Garden and Bush Keys identified at left. The larger of two boxes outlines approximate boundaries of the survey area. The smaller box delineates the most heavily sampled area.

flow pattern 27 km east of the Tortugas between Rebecca and Halfmoon Shoals attributable to strong, reversing tidal currents. These currents produce large sand waves (1–3 m in height) having crests parallel to the shelf and perpendicular to current flow. Strong southerly currents resulting from seasonal passage of storm fronts from the north and intermittent intrusions of the Loop Current (25–50 cm/s to depths of 50 or 100 m) on the shelf (Sturges, 1993) also influence the morphology of the study area.

3. Methodology

High-resolution, subbottom surveys were conducted in Southeast Channel using a special purpose, high-frequency acoustic seafloor classification system (Lambert, 1988; Lambert et al., 1993; Walter, 1998). Survey grids within a 6×6-km area were made using 4-, 12-, and 15-kHz transducers aboard two research vessels. The later two of these systems were operated using short pulse lengths (0.3 ms at 12 and 15 kHz) with narrow-beam transducers, 12° at 15 kHz and 26° at 12 kHz. Resolution using these short pulse lengths is approximately 0.15 m. The outgoing and return pulses were digitized and stored at a sample rate of 125 kHz.

The system measured real-time echo return intensity (amplitude) of time-windowed bins representing acoustic response from seafloor and subbottom sediments. Data from the upper surficial sediment bin (0.0–0.4 m) were used to calculate values of acoustic impedance estimates, co-registered with position information, and mapped in color on a computer monitor.

The 12-kHz data were obtained at a trackline spacing of approximately 1.0 km with the tracks oriented in both north/south and east/west directions. The 15-kHz data were collected over the same area with trackline spacing of approximately 150 m in a north/south direction only. A navigation plot completed in real time during the 15-kHz survey aboard the WFS *Planet* displays a colorized track of the ship that identifies the predicted acoustic impedance for the surficial (0.0–0.4 m) sediment layer (Fig. 2a).

Subbottom profiles were also presented on a color monitor as a scrolling waterfall display. Display colors represent an adjustable range of measured sound pressure level in dB per color of acoustic signal amplitude returned from the bottom and subbottom sediment volume (Fig. 3).

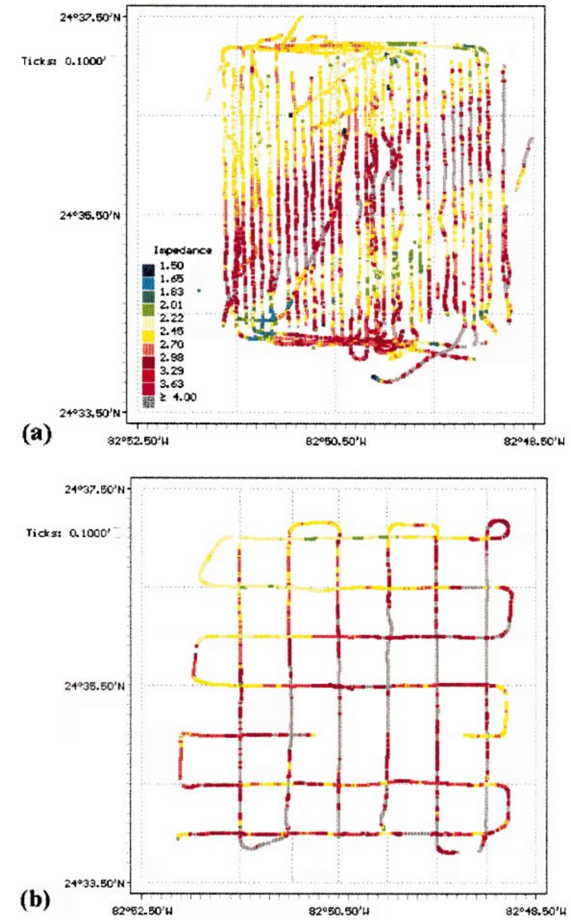

Fig. 2. (a) Colorized trackplot of surficial (upper 0.4 m) sediment acoustic impedance collected using the 15-kHz (hull-mounted) transducer aboard the WFS *Planet*. Trackline spacing is approximately 150 m. (b) Processed R/V *Johnson* trackline impedance predictions of surficial (upper 0.4 m) sediment collected using the hull-mounted 12-kHz transducer array aboard the R/V *Seward Johnson*. Trackline spacing is approximately 1.0 km. Impedance values shown in color key of a apply to both images and are reported in 10^6 kg/m^2/s. Color key (interpretation of colorized tracklines using impedance/color (*after Folk, 1974/1980): blue, low echo return (signal loss on steep slopes); green, mud* (silt size) (sand:mud ratio $<1:9$); yellow, sandy mud* (sand:mud ratio $<1:1$, may include shell); pink, muddy sand* (sand:mud ratio $>1:1$, including shell); red, sand* (sand:mud ratio $>9:1$); gray, limestone rock or coral reef.

3.1. Impedance calculations

Impedance, $Z = \rho c$, where ρ is the wet bulk density and c is the compressional wave velocity, is the most common term used to acoustically characterize a material, in this case a marine sediment. Changes of acoustic impedance indicate the amount of energy reflected from a boundary when a sound pressure wave (i.e., compressional wave) passes from a medium of one impedance to a medium of different impedance (Hamilton and Bachman, 1982).

The amplitude of reflected energy is measured by the acoustic acquisition system. These amplitudes (referred to as echo-strength) are analogous to the reflection coefficient of the upper 0.4 m of sediment beneath the seawater interface. This reflection coefficient (R) is defined as the portion of the sound pressure wave reflected off the seafloor, divided by the incident sound pressure wave impinging on the bottom; that is, the ratio of the reflected wave (P_r) to the incident wave (P_i). Therefore,

$$R = P_r / P_i \quad (1)$$

For a normal incident acoustic wave this reflection coefficient is related to acoustic impedance by the relationship,

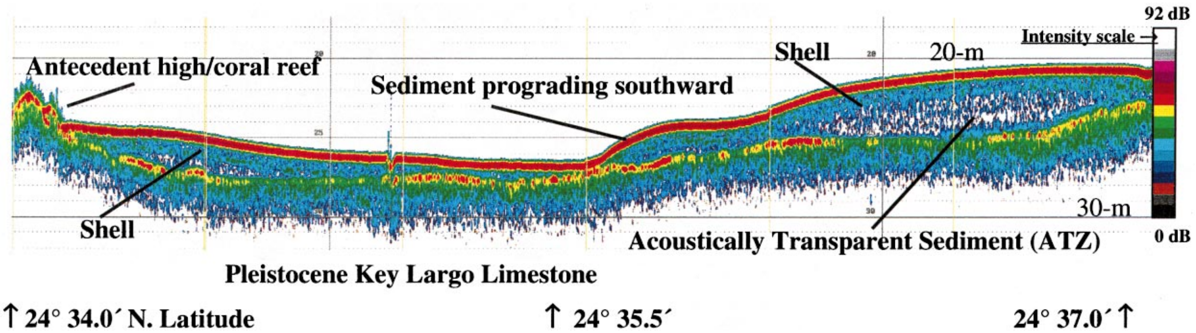

Fig. 3. Subbottom profile obtained at 4 kHz along the line nearest to Garden Key (82°52.0′W longitude). Color scale at right side indicates signal return intensity in steps of 6 dB per color (92 dB at top/white, 0 dB at bottom/black). This line is approximately 6 km long and full vertical scale is 20.0 m. Solid horizontal lines are at 5-m depth intervals. Features discussed in the text are labeled.

$$R = P_r/P_i = (\rho_2 c_2) - (\rho_1 c_1)/(\rho_2 c_2) + (\rho_1 c_1) = Z_2 - Z_1/Z_2 + Z_1 \quad (2)$$

Only a small portion of the incident energy is reflected from sediment or rock interfaces resulting in reflection coefficients of 0.5 in many cases, but typically less than 0.2 (Kearey and Brooks, 1984). The remainder is transmitted into the next medium, in this case the next layer in the sediment column. This study focuses on the response obtained from the surficial sediment bin (0.0–0.4 m) used with the 12- and 15-kHz data.

3.2. Processing acoustic data

An area covering approximately 4 km^2 in the northwest corner of the survey grid was selected for intensive study during this experiment (Fig. 1). One core site, KW-PE-GC-167 (Fig. 4), was selected to provide a ground truth reference for calibrating the acoustic system. During post-cruise processing, the 12-kHz acoustic data obtained while crossing this core site was normalized to the averaged acoustic impedance of the upper 0.4 m of the core sample values (Table 1, calibration site). After this normalization, the complete acoustic data set was processed without further system setting changes.

The 8-bit acoustic data are used with a 'calibration' file in the sediment classification software to aid in determining the structure of the subbottom and the reflectivity of the sediments within this structure. The calibration file was created on a hard sand site near Key West, Florida, prior to this study. A reference pulse created in this file was used to deconvolve the acoustic data returned from the bottom, i.e., the reference pulse is subtracted from the return pulse to compute a model of the layering structure of the sediment. However, in this application we are not concerned with the analysis of layered structure but with the surficial sediments near the sediment–water

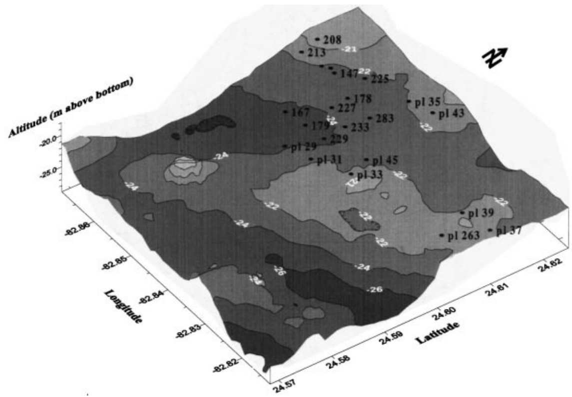

Fig. 4. Bathymetric contour map of Southeast Channel study area using altimetry data from hull mounted transducer. Contours are labeled (white) at 2.0-m intervals. Sample sites are also identified by symbol (●) and labeled in black. Bottom contours (reported as altitude in meters above bottom) are labeled in white.

Table 1
Wentworth and Folk terminology correlated with core-derived impedance, acoustic trackline predictions and predictions from impedance contour maps

Core No./calibration site	Terminology		Calculated impedance[a]	ASCS track				Contour map	
	(a) Wentworth size class	(b) Folk sand:mud ratio		Real-time		Processed		Reprocessed	
				15-kHz color	Predicted impedance range	12-kHz color	Predicted impedance (average 3 of shots)	12-kHz color	Predicted impedance range
Core No.									
208	medium/fine silt	sM	**2.73**	yellow	2.45–2.69			yellow	2.45–2.69
220	medium silt	sM	**2.64**	yellow	2.45–2.69	light yellow	2.22–2.44	yellow	2.45–2.69
210	medium/fine silt	sM	**2.67**	pink	2.70–2.97	light yellow	2.22–2.44	pink	2.7–2.97
213	medium/fine silt	sM	**2.75**	pink	2.70–2.97			yellow	2.45–2.69
147	medium silt	mS	**2.73**	yellow	2.45–2.69	yellow/red	3.11	yellow	2.45–2.69
225	medium silt	mS	**2.78**	yellow	2.45–2.69			pink	2.7–2.97
178	medium silt	mS	–	light yellow	2.22–2.44			pink	2.7–2.97
227	medium silt	mS	**2.8**	yellow	2.45–2.69			pink	2.7–2.97
179			**2.74**	yellow	2.45–2.69			red1	2.98–3.28
283			**2.81**	pink	2.70–2.97	light yellow	2.22–2.44	yellow/pink	2.45–2.97
233			**2.77**	pink	2.70–2.97	pink	2.71	pink	2.7–2.97
229				red1	2.98–3.28	red1	3.29	red1	2.98–3.28
Calibration site									
167	coarse silt	sM/mS	**2.82**	pink	2.7–2.97	pink	2.88	pink	2.7–2.97

Empty cells denote lack of data.
[a] Acoustic impedance units in 10^6 kg/m^2/s.

interface. The result of this deconvolution operation is the reflected energy level expressed as (R) in Eq. 2 above. The software uses an assumed seawater impedance of 1.5×10^6 kg/m^2/s. The remaining unknown in Eq. 2 represents the sediment impedance as Z_2.

3.3. Sedimentologic methods

Several sediment cores were collected in the northwest corner of the study site (Fig. 4). As discussed above, one of these cores, KW-PE-GC-167, was used to provide ground truth impedance calibration values for the acoustic system, whereas others were used for comparison with the real-time (15-kHz) and processed (12-kHz) impedance predictions.

Gravity cores were obtained using plastic (PVC) core barrels 3 m long with a 3-in. (7.79-cm) inner diameter and a core assembly weight of 400 lb (181.3 kg). All cores were maintained in upright positions and refrigerated while awaiting processing.

Sampling sites were selected based on data assessments from previous geologic studies of the area and by a review of normal incidence acoustic (Fig. 2a) and side-scan data (Wever et al., 1997) aboard the WFS *Planet* approximately 3 days prior to the commencement of bottom sampling by the R/V *Pelican*.

Initial analytical methods included measurements of compressional wave velocity using 400-kHz (Briggs and Richardson, 1997) and 500-kHz GEOTEK (Schultheiss and McPhail, 1989) acoustic loggers and wet bulk density by a GEOTEK multisensor core logger (Boyce, 1976; Schultheiss and McPhail, 1989). Acoustic impedance values were calculated from the product of measured sound speed and analyzed wet bulk density values.

Cores were subsampled at 2-cm intervals and analyzed for wet bulk density, and grain density using Quantachrome multi-pycnometer and ultrapycnometer-1000 helium gas pycnometers (Quantachrome Corporation, 1993). Grain-size analysis was completed on subsamples at 0.1-m intervals by pipette (Folk, 1974/1980) and sedigraph for silt and clay sizes (Briggs et al., 1996), and by sieve for larger sand and gravel (shell) sizes (Folk, 1974/1980). X-radiographs were taken of each core to delineate vertical variations in sedimentary horizons as well as to distinguish larger/dense shell fragments residing within the core sample. Additional subsamples of selected cores were dried, embedded in resin and polished for analysis by petrographic and scanning electron microscopy (Furukawa et al., 1997). Stephens et al. (1997) provide a detailed explanation of sediment processing methodologies used for all core samples.

4. Characterization of surficial sediment facies

4.1. Sediment facies patterns

Initial assessment of surficial (0.0–0.4 m) sediment type was conducted aboard the WFS *Planet* using the 15-kHz narrow-beamwidth (12°) acoustic system. Color-coded survey tracks of acoustic impedance predictions, illustrated in Fig. 2a, presented a synoptic overview of surficial facies patterns in the study area. This map provided a reference for selecting sampling sites for ground truth core and instrument deployment locations.

Several sediment types are clearly delineated on this map. Surficial sediments having acoustic impedance predictions[1] ranging between 2.45 and 2.69 i_p (yellow) dominate the northwest corner of the site. Scattered throughout portions of this sector are segments having a slightly higher impedance range (2.70–2.97 i_p, pink). The most prominent feature is the high-impedance band (red and gray segments of the tracklines) that crosses the central portion of the site from the northeast to southwest corner. This band has the highest impedance in the site, ranging from 2.98 to a maximum of 4.0 i_p and most likely represents surface exposures of limestone bedrock. Sediments in a slightly lower impedance range are also distributed intermittently throughout this section (2.70–2.97 i_p, pink). Parallel and immediately

[1] Acoustic impedance units (10^6 kg/m^2/s) are presented in an abbreviated form. Core-calculated impedance is represented by i_c and acoustically predicted impedance will use i_p.

south of the high-impedance band, lies another area of low-impedance surficial sediments, similar to those observed in the northwest sector, with impedance values ranging from 2.01 to 2.69 i_p. In the southeast section, a high-impedance bottom, 2.98 to a maximum of 4.0 i_p, again becomes more prevalent. Seemingly very low-impedance zones (blue) along several tracks are erroneous, corresponding to areas of increased acoustic scattering where bottom relief is high along angular slopes or where the seafloor surface is rough enough to cause a loss in signal return. In these areas, the narrow-beam transducer receives less of the reflected acoustic energy because it is out of the receiving window beneath the transducer.

The 12-kHz R/V *Seward Johnson* data were reprocessed to electronically calibrate the raw acoustic data with impedance values calculated from sediment bulk density and compressional wave velocity measurements at a single representative core site (KW-PE-GC-167). The raw 12-kHz data obtained at a crossing of this core location was adjusted until the same impedance value as that averaged from the upper 0.4-m increment of the core was achieved. The full data set was then reprocessed using the same system settings that were used to match the acoustic data to the core-impedance value. This process created a revised impedance trackline map that could be used to compare the real-time WFS *Planet* 15-kHz predictions (Fig. 2a) to the processed (12-kHz) predictions in Fig. 2b. The sediment facies trends that are clearly defined in the initially collected 15-kHz data are still identified in the revised data. Although the track spacing is wider in the 12-kHz survey compared to that conducted by the WFS *Planet*, similar trends in surficial sediment facies can be observed. Specifically, the northwest corner maintains the low-impedance values and the diagonal high-impedance band identified as sand and limestone rock outcrop in the initial 15-kHz interpretation remains but is represented by higher impedance levels in the revised impedance map. Thus, the calibration procedure resulted in a one-step increase in impedance estimates at the core site. The original 15-kHz WFS *Planet* data at the core site crossing recorded the track in yellow (predicted impedance of 2.22–2.69 i_p) whereas the reprocessed data was registered in pink in this region, indicating a revised impedance prediction of 2.70–2.97 i_p. Although the predicted impedance values are not exactly the same, the facies trends identified by both the processed and real-time impedance predictions are nearly identical. The most dominant surficial feature, the northeast to southwest high-impedance sand/rock belt (limestone outcrop) remains outlined as are the zones retaining lower impedance sandy muds and muddy sands.

4.2. Holocene sediment type predictions and distribution

A blanket of Holocene sediments covers a major portion of the survey area except to the east where the Key Largo limestone is emergent and in the southern sector where antecedent highs and patch reefs are common (Mallinson et al., 1997). Sediment thickness varies from less than 1 m in the northeast to greater than 3 m in the northwest. Sediment thickness in the bedrock depressions at the base of the antecedent high formations in the south range between 3 and 5 m. Average sediment thickness in the extensively sampled study area is about 2 m. Recent sediments are presently being deposited along the base of the eastern escarpment between Bush Key and Long Reef at the northwest corner of the study site, creating a gently sloping sediment embankment of mixed carbonate silt, sand, and shell. This thick deposit seems to be prograding in a southerly direction as indicated by the toe of sediment located near 24°35.5′N latitude on the western-most acoustic trackline along 82°52.0′W longitude (Fig. 3). This apparently is a transitional zone of muddy sands (pink, predicted impedance of 2.70–2.97 i_p) lying between a thick sequence of sandy muds (yellows, predicted impedance of 2.22–2.69 i_p) to the north and a thin veneer of coarse sand and gravel sizes (red, predicted impedance of 2.98–3.99 i_p) to the south. These coarse sediments thicken further to the south where they ultimately coincide with a bedrock outcrop as it transitions into the antecedent high formation. These deposits are comprised of broken shell and coral fragments that have been

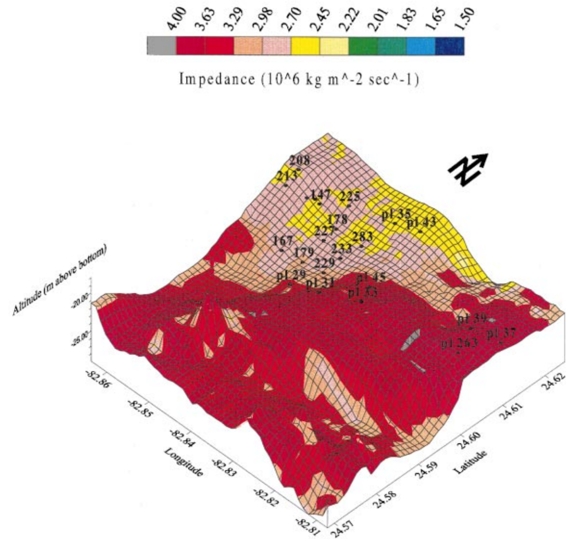

Fig. 5. Predicted acoustic impedance contour map of surficial sediment cover in Southeast Channel study area using 12-kHz reprocessed data from R/V *Seward Johnson*. The contour map is draped over the 3-D bottom reported as altitude in meters above bottom.

removed from and transported off the banks to the west and the antecedent highs in the south (Mallinson et al., 1997).

Interpreted surficial sediment types are identified in the trackline impedance maps presented in Fig. 2. These sediments consist of soft, carbonate muds (M, green) and sandy muds (sM, light yellow) having impedances ranging between 2.01 and 2.44 i_p, soft carbonate muddy sands (mS, yellow and pink) having impedances ranging between 2.45–2.97 i_p, and hard, fine to coarse sands (fmS and mcS, red) having impedances ranging between 2.98 and 3.99 i_p. High-impedance zones (4.00 i_p), illustrated in gray, delineate limestone rock exposures or coral reefs.

Topographic lows in the bedrock further to the south, provide additional repositories for sedimentary materials in this area. These sediment ponds are situated on the north and south flanks of topographically high (2–5 m relief), live coral-gal reef structures. These structures form in a southwest to northeast diagonal band across the southern portion of the study area. Up to 5 m of Holocene sediments have been deposited in these bedrock lows.

Fig. 5 displays 12-kHz color-contoured surficial sediment property predictions co-registered with the three-dimensional (hull-mounted) transducer altimetry. The thick sediment cover in the northwest corner is somewhat constrained by the dominant northeast to southwest high-impedance surface. Also observed on this illustration is the rough (karst) bottom in areas having coarse sediments and the prominent antecedent high structure with associated patch reefs in the southwest and southeast sectors.

4.3. Bottom samples

4.3.1. Acoustic impedance/mean grain size and size–frequency distribution

The average acoustic impedance value of 2.82 i_c representing the upper sediment column (0.0–0.4 m) at core site KW-PE-GC-167 was used as the ground truth reference value for 'calibrating' the acoustic 12-kHz system (Table 1). Average mean

Table 2
Average of core calculated acoustic impedance (upper 0.4 m), acoustic system-predicted impedance (two frequencies), percent size fraction and mean grain size near listed core locations

Core No.	Acoustic impedance (10^6 kg/m^2/s)					% Size fraction			
	Core	15-kHz	Δ	12-kHz	Δ	Sand	Silt	Clay	Phi
147	2.73	2.69	−0.04	3.11	0.38	32	47	20	5.6
233	2.77	2.9	0.13	2.71	−0.1	no data			
229	no data	2.86	n/a	3.29	n/a	no data			
225	2.78	2.76	0.02	no data	n/a	34	43	21	5.9
178	no data	2.95	n/a	no data	n/a	34	47	18	5.3
227	2.8	2.67	−0.13	no data	n/a	34	46	19	5.6
179	2.74	2.74	0.00	no data	n/a	no data			

grain size for this site was 4.9 phi (0.033 mm), classifying the sediment in Wentworth (1922) terms as coarse silt (Table 2).

Weight percent frequency distribution for this core, however, was nearly equal in the sand and silt sizes at 41 and 39%, respectively, with 17% in the clay size and approximately 3% in the gravel fraction. Also identified in Table 1 are the color of the acoustically predicted impedance contour in Fig. 5 near core site KW-PE-GC-167 (pink) and the representative predicted acoustic impedance range for this color (2.70–2.97 i_p).

Calculated acoustic impedances from seven additional core sites in the northwest corner, as well as acoustic impedance predictions obtained at track locations near them, are presented in Table 2. Also presented in this table are the size fraction (%) and mean grain size (phi) for the upper 0.4 m of each core. The majority of bottom samples were obtained from the northwest corner of the site because sediment cover in other areas to the east and southeast was much thinner and consisted of more granular materials. These hard-bottom areas, illustrated in the red contoured areas in Fig. 5, were nevertheless sampled with bottom grab samplers. Data from these samplers, reported by Wever et al. (1997) are presented in Table 3.

Core sites selected for this work (Fig. 4) were used because they lie near or along the acoustic tracklines (Fig. 2). Cores KW-PE-GC-208 and 213 are located near the western-most line transited by the R/V *Seward Johnson*. Averaged impedance values for these core sites are 2.73 and 2.75 i_c, respectively. Mean grain sizes at these sites are 6.5 and 6.4 phi, respectively, in the medium to fine silt class. Approximately 300 m to the east, cores KW-PE-GC-210 and 220 have lower impedance values of 2.67 and 2.64 i_c. Mean grain size is 6.4 phi at sites 210, 208 and 213 to the west. Mean grain size is slightly coarser at site 220 at 5.9 phi. The sand-size fraction at all four of these sites is less than 22%, with a dominant combined silt- and clay-size fraction of 80%.

About 250 m to the east, core KW-PE-GC-147 has an average measured impedance value close to those identified above at 2.73 i_c. However, mean grain size at this site decreases to 5.6 phi (medium silt) as the portion of sand-size particles increases to about 30% with a corresponding decrease in the silt/clay size fraction to about 70%.

Cores collected along a line 300 m east (KW-PE-GC-225, 227, and 179) have surficial average impedance values of 2.78, 2.80, and 2.74 i_c, respectively. No surficial impedance value is available for core 178 because no sound velocities were obtained in the top portion of the core. Mean grain size values were 5.9 phi for core KW-PE-GC-225, 5.3 for core KW-PE-GC-178 and 5.6 for core KW-PE-GC-227, all falling within the me-

Table 3
Wentworth terminology as applied by Wever et al. (1997) to selected ground truth sediment samples

Grab No.	Terminology			Contour map	
	Wentworth size class	Real-time		Processed	
		15-kHz color	Predicted impedance range[a]	12-kHz color	Predicted impedance range[a]
pl 29	medium/fine silt	red1	2.98–3.28	red2	3.29–3.62
pl 35	medium/fine silt			dark yellow	2.45–2.69
pl 31	medium/fine silt	red1	2.98–3.28	red3	3.63–3.99
pl 43	medium/fine silt	yellow	2.45–2.69	dark yellow	2.45–2.69
pl 45	medium/fine silt	yellow	2.45–2.69	red2	3.29–3.62
pl 33	medium/fine sand	red/gray	> 3.63	red3	3.63–3.99
pl 39	medium/fine sand	red/gray	> 3.63	red3	3.63–3.99
pl 37	medium/fine sand	red/gray	> 3.63		
pl 263	coarse/medium sand	gray	> 3.99	red3	3.63–3.99

Samples are compared to pertinent real-time and reprocessed acoustic impedance predictions obtained along tracklines and from contour maps. Empty cells denote lack of data.

[a] Acoustic impedance units in 10^6 kg/m^2 s^{-1}.

dium silt category. No grain size or weight percent distribution was completed for core KW-PE-GC-179. Size distribution in these sediments remained dominated by the silt/clay fractions at an average of 65% while sand-size contribution increased to about 34%.

The last group of three cores used for this study (KW-PE-GC-229, -233, and -283) were obtained along 82°51.0′W where both the R/V *Seward Johnson* and the WFS *Planet* crossed near these sites. The surficial impedance value for core KW-PE-GC-233 was 2.77 i_c and that of core KW-PE-GC-283 was 2.82 i_c. No surficial impedance value is available for core KW-PE-GC-229. Neither grain size nor frequency distributions are available for any of these three sites.

4.3.2. Biogenic components

The most dominant species represented in these sediments is the calcareous green alga *Halimeda* in varying states of diagenesis within the sediment column (Furukawa et al., 1997; Mallinson et al., 1997). Stephens et al. (1997), in their analysis of cores in the area, reported a minimal amount of small shells in the upper fine portion (<5 phi) of the sediment column between 0.9 and 1.4 m below seafloor (mbsf), varying with geographic location. These shelly horizons are indicated in the interpretations of the acoustic profile in Fig. 3. Below this level, sediment structure and content changes to a somewhat desiccated, shelly lag layer averaging between 0.0 and 0.4 m in thickness. Coarse molluscan shells consisting of partial and broken gastropods and pelecypods and coral debris dominate this horizon. The sediments below this shell deposit and in the deepest cores consist of a bioturbated layer of fine-grained (<6.5 phi) gray sandy mud. Lithified and unlithified burrows were common in the upper and lower portions of the sediment cores, but not necessarily in the coarse lag deposits near intermediate depths. D'Andrea and Lopez (1997) concluded that these burrows were created mostly by polychaetes and callianassid shrimp. This bioturbaceous activity effectively removes the primary micro- and macro-stratigraphic structure in the upper sediment column leaving fossilized burrows in its place.

Images obtained by scanning electron microscope confirm the predominance of *Halimeda* plates and aragonite needles in these sediments (Furukawa et al., 1997). Fig. 6 illustrates the micro-structural components of the upper sediment column (0.2 and 0.64 mbsf) obtained from KW-PE-GC-147, located in the low-impedance yellow area of Fig. 2a. Wet bulk density and compressional wave velocity at this site are 1.80 g/cm^2 and 1506 m/s, respectively. Mean grain size is 5.6 phi and the size distribution includes 32% sand, 47%

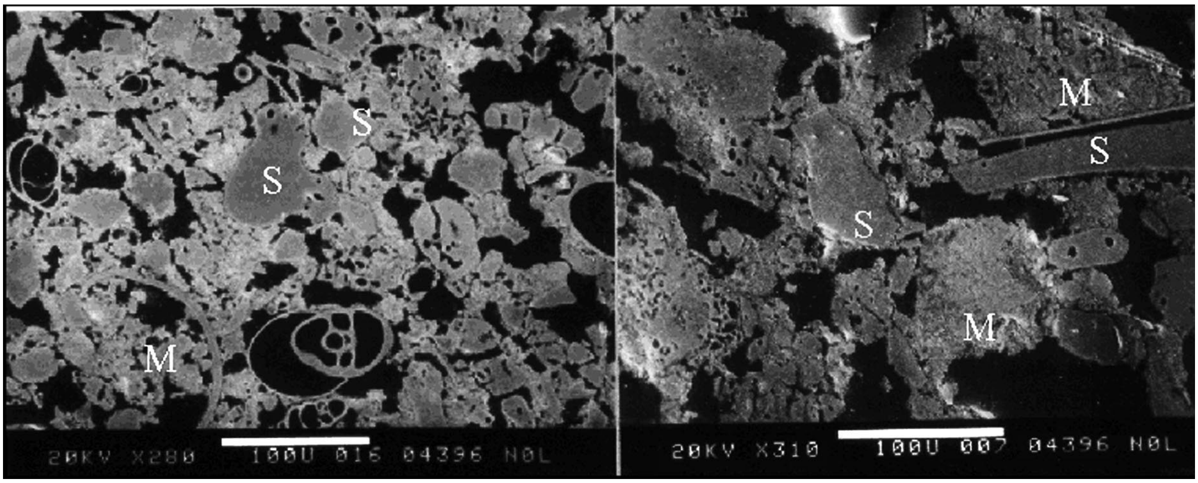

Fig. 6. Scanning electron microscope images of subsamples from core KW-PE-GC-147. Large and small *Halimeda* platelets (S) are smooth and fine-grained (silt size), whereas particle aggregates (M) are cloudy with less well defined edges. Left sample is from 0.2 m and the one at the right 0.65 mbsf. Scale bar: 100 µm. (After (Furukawa et al., 1997.)

silt and 20% clay. Skeletal grains appear smooth and similar to the grain labeled (S) in this image. Cloudy and/or shiny portions (labeled M) are indicative of fine-grained micritic particle aggregates that form by mechanical and chemical alteration of the coarse platelets (Furukawa et al., 1997).

4.4. Determination of facies units

Wentworth and Folk classification terminologies, based on mean grain size and percent size class respectively, are presented in Table 1 along with calculated acoustic impedance values and the predicted impedance values obtained from the acoustic tracks and contour maps. The calibration site (KW-PE-GC-167) has the highest calculated impedance and the coarsest grain size of all cores (phi = 4.9). This core is classified in terms of mean grain size (after Wentworth) as coarse silt and in terms of sand:mud ratio (after Folk) as either sandy Mud or muddy Sand. All other cores have mean grain sizes greater than 5.3 phi, classifying them in either medium silt (those up to 5.9 phi) or medium to fine silt (those above 5.9 phi) size ranges. Cores obtained at the western-most side of the area (Fig. 4, KW-PE-GC-208, 210 and 213) have the finest mean grain size. These three cores also classify in Folk terms as sandy muds, whereas the others, except for core KW-PE-GC-220, classify as muddy sands. Folk (1974/1980) classified all grain sizes with phi >4.0 in either silt- or clay-size fractions and further describes them all in a range identified as mud. This illustrates that all of the calculated acoustic impedances in the range of 2.64–2.82 i_c can be classed as muds. Breaking this range into two components, the record shows (Table 1) that sM fall below an impedance of 2.73 i_c, whereas mS have impedances above 2.73 i_c. Core KW-PE-GC-147, although having an impedance of 2.73 i_c, is classified as mS in the table because it has a higher percentage of sand than others at or below 2.73 i_c. No core data are available to develop the correlation between measured acoustic impedance and sediment type in the sand and limestone hard-bottom areas. Therefore, sediment-type descriptions from four grab sample sites collected by Wever et al. (1997) in the eastern portion of the

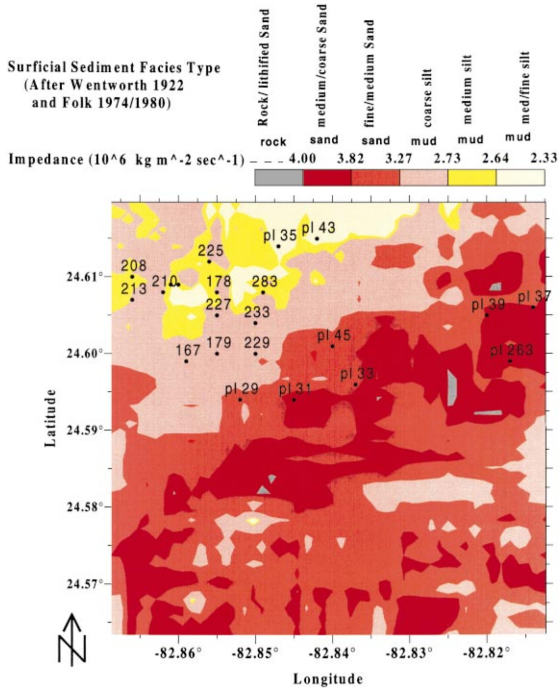

Fig. 7. Two-dimensional, acoustically predicted, surficial sediment facies contour map. Sample locations are indicated. Contours are based on predicted acoustic impedance. Facies terminology in key at top was associated with pertinent impedance values in Tables 1 and 3. These associations are based on correlation of core-derived impedance, mean grain size and sand:mud ratio presented in Tables 1–3. Sample locations are also identified.

study site (pl 33, 37, 39, and 263) were used (Table 3) to define the upper limits of the impedance vs. facies relationship. For the rock description, an assumption was made that acoustic impedance for rock is greater than that of sand and that the sea floor with exposed rocky areas was relatively flat with minimal angular relief.

Fig. 7 presents the result of adjusting the color bands in the contour software to match the relationships identified in Tables 1 and 3. This illustration provides a new and informative view of the study area in which color contours represent the facies identified in the legend. Facies nomenclature is modeled after Wentworth's categorization in relation to grain diameter and Folk's classification based on sand:mud ratio. This contour map displays sediments in the northwest corner consisting of fine to coarse silts with a coarsening trend to the east represented by the sedimentary changes identified by varying sand size descriptions. Also noted on this map are the areas where the Key Largo limestone is exposed on the bottom and the areas identified as coral reef structures. The application of this methodology is limited in the hard-bottom areas due to lack of ground truth data from these areas. In particular, the occurrence and extent of the exposed bedrock are not appropriately represented after extrapolating the impedance vs. sediment type based solely on four grab samples in the hard-bottom area. Walter et al. (1997) and Walter (1998) presented 4-kHz subbottom profiles across the entire site that reveals the exposed bedrock at several locations. Wever et al. (1997) using side scan imagery reported the exposed bedrock as 'new reef' structure and Mallinson et al. (1997) identified these as 'hardbottom and coarse sediment' areas.

5. Discussion

5.1. Facies analysis

The 15-kHz predicted acoustic impedance trackline map created in real time aboard the WFS *Planet* provides a reasonable estimation of the distribution of surficial sediment types in the survey area. These sediment facies are comprised of carbonate muds and sands in varied proportions, particularly in the sandy-silt and silty-sand size classes. Additional bottom facies that play an important role in the morphology of the area are limestone rock and coral reefs.

These classifications were made during the initial WFS *Planet* survey by evaluating the trackline acoustic impedance predictions (Fig. 2a) in combination with vertical acoustic profiles similar to that of Fig. 3. Many of these profiles record a high-impedance subbottom reflector, the Pleistocene surface, which crops out in several locations in the east and transitions into a topographically high-reef structure in the south (Mallinson et al., 1997; Walter et al., 1997; Walter, 1998; Wever et al., 1997). Little, if any, sediment cover is observed at these locations. Sediment cover does, however, thicken towards the north and west on approaching the shallow carbonate banks of the Dry Tortugas (Mallinson et al., 1997, fig. 3C).

The area is portrayed in the 15-kHz trackline plot (Fig. 2a) and the 12-kHz trackline plot (Fig. 2b) in yellow as the sector with the lowest impedance ($< 2.45\ i_p$). The low-impedance return occurs here because acoustical backscatter is reduced as the result of the apparent dominance of fine materials in the sediment volume. This observation is corroborated by the presence of low acoustic impedance values calculated from core-derived wet bulk density and compressional wave velocities, low mean grain sizes and a predominance of silt- and clay-size fractions (Tables 1 and 2).

The central north and northwest sections have a thick sediment covering of a carbonate silt/sand mixture, while the hard, sometimes exposed limestone bedrock is a prevalent feature that crosses the test area diagonally from the northeast to the southwest. Low-impedance/soft silty Holocene sediment ponds that overlie the buried limestone bedrock lows between antecedent high structures represent the southern portion of the test area.

Deep sediments in the sediment ponds, as well as other thick (> 3 m) sediment deposits in the northwest corner of the study area, display a distinctly weak acoustic signature and are described as 'acoustic transparent zones' (ATZs). These zones are ostensibly devoid of acoustic return below the sequence of carbonate sediments above them. The low-intensity acoustic return is observed best in the 4-kHz acoustic imagery by a white zone that lies below the surficial sediment and slightly above the bedrock surface (Fig. 3). The location of these ATZs in the northwest corner correlates well with a change in mean grain size and color in several of the cores that penetrated to this depth. The low-acoustic response also coincides with the occurrence of darkening sediment color (graying) and fine grain size (silt) at core sample depths below approximately 2 m within the study area (Mallinson et al., 1997; Stephens et al., 1997).

The impedance contour maps presented in Figs. 5 and 7 were created after reprocessing the R/V *Seward Johnson* 12-kHz acoustic data. Comparisons of the 12-kHz trackline data with the contour maps illustrate reasonable agreement. Sediment facies trends characterized in these maps are comparable to the uncorrected (real-time) 15-kHz data. However, portions of the detailed data in the corrected (12-kHz) trackline map (Fig. 2b), denoting a more heterogeneous and spatially variable sediment facies distribution, are lost in the process of contouring the data due to the interpolations performed by the gridding software. Apparently the spatially detailed coverage obtained on a ping-to-ping basis by the acoustic system and conspicuous in Fig. 2b, is averaged out during the process of gridding and contouring the data, especially at wide track spacing (1.0 km) used during acquisition of the 12-kHz data.

A comparison of acoustic impedance values from sediment core data with 12- and 15-kHz acoustic predictions in the northwest quadrant of the study area show close agreement (Table 2). The processed track data presented in Table 1 represent an average value for three consecutive pings at the closest point to the core site. In most cases, the acoustic track did not cross over the core location exactly and, as observed in the color trackline impedance plots, surficial sediment impedances were variable in several cases along track. The slight discrepancy in the 12-kHz predictions is due to the fact that no sensitivity information was available regarding the 12-kHz, hull-mounted transducer array. This information is a required input to the acquisition software to provide accurate raw data values from which the sediment impedance predictions are calculated (Lambert, 1988).

No core data are available to test the validity of the acoustic predictions in the red and gray regions of the contour maps. However, Wever et al. (1997) reported Wentworth size class descriptions for four grab samples obtained in this area (locations identified with 'pl' preceding the site ID number in Fig. 4) as well as five additional samples obtained from the northwest corner. A total of 31 samples were described by Wever et al. (1997) using Wentworth terminology. Four size classes were identified within the entire study area: fine and medium silt, coarse silt, fine and medium sand, and coarse sand. Both silt sizes were prevalent in the northwest corner while sands were dominant in the eastern area of the site. These data are presented in Table 3 with predicted acoustic impedance ranges (colors) at these sites (site #167 was also used by Wever but is reported in Table 1). Side scan sonar records illustrating areas of high and low backscatter also confirm the trend from coarse sediment cover in the east to fine cover in the west (Wever et al., 1997). The acoustic facies identified using side scan sonar data compare reasonably well with facies delineated by the trackline maps (Fig. 2) and the impedance contour maps presented in Figs. 5 and 7.

5.2. Geologic assessment

Sediments in the experimental site consist almost entirely of carbonate materials with $< 10\%$ terrigenous content (Briggs et al., 1996; Stephens et al., 1997). The major source of silt and sand size fractions in the locations with thick sediment cover are the benthic, calcareous green alga *Halimeda* transported off the shallow platforms adjoining the Keys (Halley, 1979; Bentley and Nittrouer, 1997).

A scanning electron microscope image of two subsamples from core KW-PE-GC-147 (Fig. 6) shows a typical breakdown of constituent particles within the sediment volume. Particularly evident in this and other samples are the skeletal grains of sand- and silt-sized *Halimeda* fragments with interstitial, fine-silt-sized, micritic aggregates. The source of these *Halimeda* skeletons is the carbonate banks to the west, north and northeast of the study area, reported by Vaughan (1914), Shinn et al. (1977), Halley (1979), and recently by Bentley and Nittrouer (1997).

All geomorphic features in this area have a northeast to southwest trend suggesting the presence of a prevalent current pattern that flows around the platform from north and northeast and the southwest (Wright et al., 1997). Accounting for the bathymetric features within the confines of the immediate Southeast Channel area, these current patterns result in a retention of sedimentary material at the foot of the eastern escarpment of the Garden and Bush Key platform. Besides tidal current influences, the dominance of subtropical easterly winds likely create an additional constraint on transport of sediment out of this area (Rhodes et al., 1989), enhancing the potential for retention of sediment.

Exposures of limestone bedrock and coral reef communities are also apparent in several sections of the study area. The reefs occur on bathymetric highs formed by the ascending bedrock in a northeast-to-southwest diagonal band across the southern portion of the study area. Thick sediment ponds have accumulated on the flanks of these features.

Signs of paleo-subaerial exposure and paleo-current effects are indicated by the presence of several karst features on the exposed and buried limestone bedrock (Figs. 8 and 9, respectively). Mallinson et al. (1997) also recognized karst on the surface of the Key Largo limestone bedrock. These features suggest that previously active processes eroded the buried bedrock formation during a period of lowered sea level. Walter et al. (1997) and Walter (1998) showed evidence of an incised paleo-channel illustrated in several acoustic records crossing the site from west to east. This feature appears as a sharp ‘V’ trending downdip along the Pleistocene bedrock surface and eastward through the study area, suggesting a somewhat linear northeast-to-southwest channel (Fig. 9). Interestingly, this paleo-channel also has an inclination similar to that of the present reef structure, i.e., northeast to southwest.

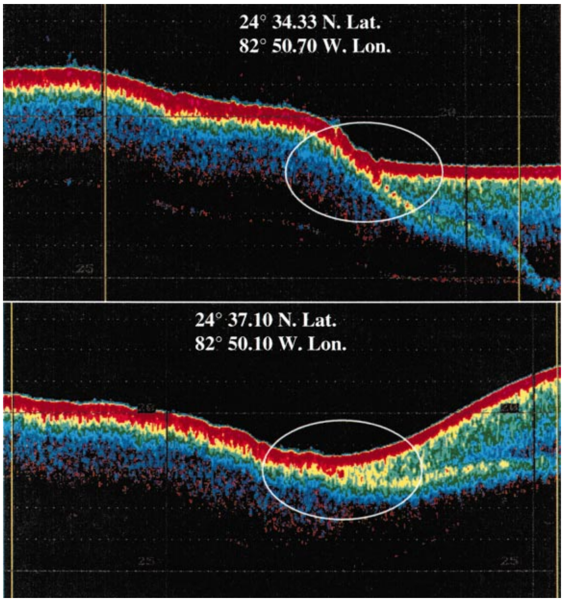

Fig. 8. Acoustic imagery showing examples of locations (white ellipses) where Pleistocene Key Largo Limestone crops out onto the seafloor. Positions are approximate.

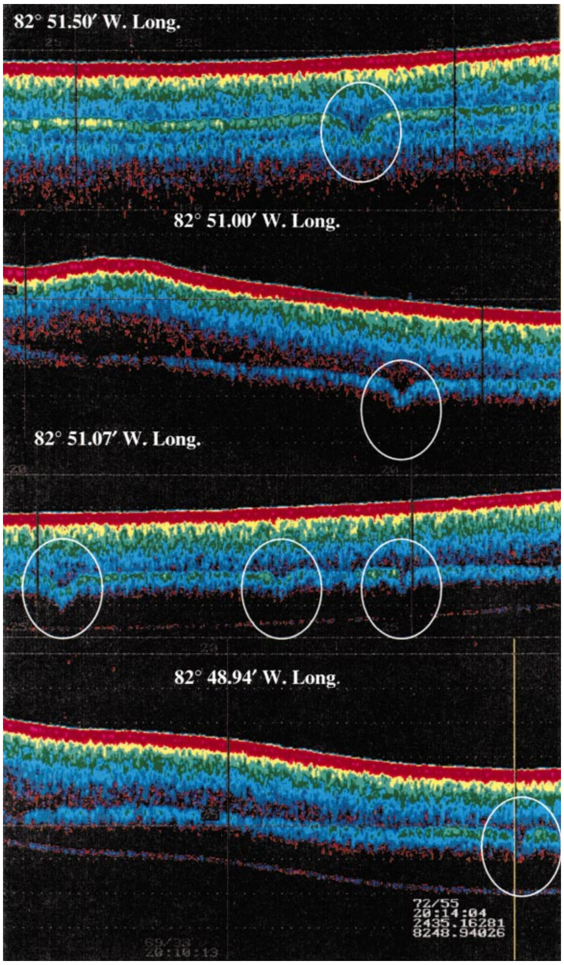

Fig. 9. Acoustic imagery showing incised features (white ellipses) extending eastward through a portion of the study site in the buried Pleistocene surface. Positions are approximate.

6. Conclusions

The combined analysis of core and acoustic data from Southeast Channel shows a variety of bottom facies provinces ranging from hard corals in the southern portion to soft carbonate sandy silts and silty sands in the regions with thick sediment cover (> 3 m). The northwest corner, adjacent to Garden and Bush Keys, has approximately 1–3 m of silty sand (with a shell layer approximately 1 mbsf) over the Key Largo limestone bedrock. As this sediment layer thins over the bedrock to the east, it transitions into a mixture of coarser silty sand and shell. Thick sequences of carbonate silts have also been deposited in the topographic lows of the limestone bedrock at the flanks of the reefs. All of these thick sequences exhibit a low-intensity acoustic response, i.e., are acoustically transparent, at approximately the same depth below seafloor as the graying/finer sediments observed in core samples.

Carbonate bedrock underlies the surficial sediments in the entire area, but rises to the seafloor and crops out in the northeast corner of the study area. This bedrock also crops out at the southern portion, partitioning into two separate carbonate reef structures that pass through the southern portion of the site in a northeast-to-southwest direction. The areas of bedrock outcrop are devoid of significant sediment cover but may retain coarse sand- and gravel-size fractions.

Correlation of two independently collected acoustic data sets (Fig. 2a, 15 kHz at 150-m spacing and Fig. 2b, 12 kHz at 1-km spacing) demonstrates the advantage of producing a real-time impedance map to represent bottom composition and structure within the boundaries of a surveyed area. Normalizing the sediment acoustic impedance data at the same position as that of a ground truth core sample yields predictions that fall within an acceptable range of accuracy to define sediment facies in terms of combined Wentworth/Folk descriptions, i.e., mean grain size and text-based sediment type. The approach of correlating acoustic impedance values with sediment mean grain size and percent size fraction can be used with confidence to construct a surficial sediment facies map to characterize sediment facies and delineate their areal distribution. Two- and three-dimensional impedance contour maps created with this data provide a representative and usable illustration of sediment facies patterns, provided adequate coverage is obtained with an appropriate survey pattern.

Acknowledgements

Funding for this work was provided by the Office of Naval Research/Coastal Benthic Boundary Layer/Special Research Program (Dr. Michael D. Richardson, Program Manager) and the Mine Countermeasures Tactical Environmental Data Systems Project (Mr. Samuel Tooma, Program Manager). We also wish to thank Dr. Herb Eppert, Superintendent/Marine Geosciences Division/Naval Research Laboratory, for his support. We are grateful to the National Park Service for permitting this study in Dry Tortugas National Park. The primary author expresses his sincere appreciation to Dr. Gary Zarillo (Florida Institute of Technology) for his inspiration in pursuit of this work, and for his guidance and encouragement over the years. We are extremely grateful to Dr. Dawn Lavoie for providing much needed direction, encouragement and constructive critique while conducting this work. We thank Sean Bailey for analyzing the cores, Kevin Stephens for compiling and providing access to the sediment property data, and Yoko Furukawa for use of the SEM images. We wish to thank the captain, officers and crew of the WFS *Planet* and R/V *Johnson* for their assistance in acquiring the acoustic and core data and Dr. Thomas Wever (FWG) and Dan Lott who provided excellent support as chief scientists. We are grateful to Rick Mang and Bill Sawyer for their logistics and navigation help during the fieldwork. The NRL contribution number is NRL/JA/7431-99-0011.

References

Bathurst, R.G.C., 1975. Carbonate Sediments and Their Diagenesis, 2nd ed. Elsevier, Amsterdam, 620 pp.

Bentley, S.J., Nittrouer, C.A., 1997. Environmental influences on the formation of sedimentary fabric in a fine-grained carbonate-shelf environment: Dry Tortugas, Florida Keys. Geo.-Mar. Lett. 17 (4), 268–275.

Boyce, R.E., 1976. Definitions and laboratory techniques of compressional sound velocity parameters and wet-water content, wet bulk density, and porosity parameters by gravimetric and gamma ray attenuation techniques. In: S.O. Schlanger (Ed.), Initial Reports Deep Sea Drilling Project 33, Appendix I. US Government Printing Office, Washington, DC, pp. 931–958.

Briggs, K.B., Richardson, M.D., 1997. Small-scale fluctuations in acoustic and physical properties in surficial carbonate sediments and their relationship to bioturbation. Geo.-Mar. Lett. 17, 306–315.

Briggs, K.B., Lavoie, D.L., Stephens, K.P., Richardson, M.D., Furukawa, Y., 1996. Physical and geoacoustic properties of sediments collected for the Key West Campaign, February 1995: A data report, NRL/MR/7431-96-8002, Naval Research Laboratory, Stennis Space Center, MS, 395 pp.

D'Andrea, A.F., Lopez, G.R., 1997. Benthic macrofauna in shallow water carbonate sediment: major bioturbators at the Dry Tortugas. Geo.-Mar. Lett. 17, 276–282.

Davis, R.A., 1983. Depositional Systems, A Genetic Approach to Sedimentary Geology. Prentice-Hall, Englewood Cliffs, NJ, 669 pp.

Dunham, R.J., 1962. Classification of carbonate rocks according to texture. In: W.E. Ham (Ed.), Classification of Carbonate Rocks. Am. Assoc. Petrol. Geol. Mem. 279, 108–121.

Enos, P., 1974. Surface Sediment Facies of the Florida-Bahamas Plateau. Geological Society of America Map, 5 pp.

Folk, R.L., 1974/1980. Petrology of Sedimentary Rocks. Hemphills, Austin, TX, 170 pp.

Ford, J., Wayland, R., Waddell, E., Hamilton, B., 1988. Meteorological database and synthesis for the Gulf of Mexico. MMS OCS Study MMS 88-0064. Unpublished technical report, US Department of the Interior, New Orleans, LA, 226 pp.

Furukawa, Y., Lavoie, D., Stephens, K.P., 1997. Effect of biogeochemical diagenesis on the sediment fabric in shallow marine carbonate sediments near the Dry Tortugas, Florida. Geo.-Mar. Lett. 17, 283–290.

Halley, R.B., 1979. Guide to Sedimentation for the Dry Tortugas. Southeastern Geol. Soc. Publ. 21, Tallahassee, FL, 99 pp.

Hamilton, E.L., Bachman, R.T., 1982. Sound velocity and related properties of marine sediments. J. Acoust. Soc. Am. 72, 1891–1904.

Kearey, P., Brooks, M., 1984. An Introduction to Geophysical Exploration. Blackwell Scientific Publications, Oxford, 296 pp.

Lambert, D.N., 1988. An evaluation of the Honeywell ELAC computerized sediment classification system. NORDA Report 169, Naval Research Laboratory, Stennis Space Center, MS, 53 pp.

Lambert, D.N., Cranford, J.C., Walter, D.J., 1993. Development of a high resolution acoustic seafloor classification survey system. Proc. Inst. Acoust. Bath 15, 149–156.

Mallinson, D., Locker, S., Hafen, M., Naar, D., Hine, A., Lavoie, D., Schock, S., 1997. A high-resolution geological and geophysical investigation of the Dry Tortugas carbonate depositional environment. Geo.-Mar. Lett. 17, 237–245.

Murphy, L.E. (Ed.), 1993. Dry Tortugas National Park, Submerged Cultural Resources Assessment. National Park Service, Santa Fe, NM, 434 pp.

Quantachrome Corporation, 1993. Ultrapyncnometer Users Manual. Boynton Beach, FL.

Rhodes, R.C., Thompson, J.D., Wallcraft, A.J., 1989. Buoy-calibrated winds over the Gulf of Mexico. J. Atmos. Oceanogr. Technol. 6, 608–623.

Schultheiss, P.J., McPhail, S.D., 1989. An automated P-wave logger for recording fine scale compressional wave velocity structures in sediments. In: W. Ruddiman, M. Sarnthein (Eds.), Proc. ODP Sci. Results. ODP, pp. 407–413.

Science Applications, Inc., 1987. Gulf of Mexico physical oceanography program, final report, year 4, Vol. 2. OCS study, MMS 87-0007, unpublished technical report. Science Applications International Corp. (SAIC), Raleigh, NC, 226 pp.

Shinn, E.A., Hudson, J.H., Halley, R.B., Lidz, B.H., 1977. Topographic control and accumulation rate of some coral reefs: South Florida and Dry Tortugas. In: R.B. Halley (Ed.), Guide to Sedimentation for the Dry Tortugas. Southeastern Geol. Soc. Publ. 21, Tallahassee, FL, pp. 90–96.

Shinn, E.A., Holmes, C.W., Hudson, J.H., Robbin, D.M., Lidz, B.H., 1982. Non-oolitic, high energy carbonate sand accumulations – the Quicksands, southwest Florida Keys. Am. Assoc. Pet. Geol. Bull. 66, 629–630.

Shinn, E.A., Lidz, B.H., Holmes, C.W., 1990. High-energy carbonate sand accumulation, the Quicksands, southwest Florida Keys. J. Sediment. Petrol. 60, 952–967.

Stephens, K.P., Fleischer, P., Lavoie, D.L., Brunner, C., 1997. Scale dependent physical and geoacoustic property variability of recent, shallow-water carbonate sediments from the Dry Tortugas Keys, Florida. Geo.-Mar. Lett. 17, 299–305.

Sturges, W., 1993. Dry Tortugas physical oceanography. In: Murphy, L.E. (Ed.), Dry Tortugas National Park, Submerged Cultural Resources Assessment. National Park Service, Santa Fe, NM, pp. 27–49.

Vaughan, T.W., 1914. The building of the Marquesas and Tortugas atolls and a sketch of the geologic history of the Florida reef tract. Carnegie Inst. Washington 5, 57–67.

Walter, D.J., 1998. Sediment Facies Determination Using Acoustic Techniques in a Shallow-water Carbonate Environment Dry Tortugas, Florida. M.S. Thesis, Florida Institute of Technology, Melbourne, FL, 118 pp.

Walter, D.J., Lambert, D.N., Young, D.C., Stephens, K.P., 1997. Mapping sediment acoustic impedance using remote sensing acoustic techniques in a shallow-water carbonate environment. Geo.-Mar. Lett. 17, 260–267.

Wentworth, C.K., 1922. A scale of grade and class terms for clastic sediments. J. Geol. 30, 377–392.

Wever, T.F., Fiedler, H.M., Fechner, G., Abegg, F., Stender, I.H., 1997. Side-scan and acoustic subbottom characterization of the sea floor near the Dry Tortugas, Florida. Geo.-Mar. Lett. 17, 246–252.

Wright, L.D., Friedrichs, C.T., Hepworth, D.A., 1997. Effects of benthic biology on bottom boundary layer processes, Dry Tortugas Bank, Florida Keys. Geo.-Mar. Lett. 17, 291–298.